ARL-SR-0346 • OCT 2015

US Army Research Laboratory

Characterization of a Reverberation Chamber

by Andrew J Klinkowski

NOTICES

Disclaimers

ARL-SR-0346 ● OCT 2015

US Army Research Laboratory

Characterization of a Reverberation Chamber

by Andrew J Klinkowski
Sensors and Electron Devices Directorate, ARL

REPORT DOCUMENTATION PAGE

Form Approved
OMB No. 0704-0188

1. REPORT DATE *(DD-MM-YYYY)*
October 2015

2. REPORT TYPE
Special report

3. DATES COVERED (From - To)
06/2015–08/2015

4. TITLE AND SUBTITLE
Characterization of a Reverberation Chamber

5a. CONTRACT NUMBER

5b. GRANT NUMBER

5c. PROGRAM ELEMENT NUMBER

6. AUTHOR(S)
Andrew J Klinkowski

5d. PROJECT NUMBER

5e. TASK NUMBER

5f. WORK UNIT NUMBER

7. PERFORMING ORGANIZATION NAME(S) AND ADDRESS(ES)
US Army Research Laboratory
ATTN: RDRL-SER-M
2800 Powder Mill Road
Adelphi, MD 20783-1138

8. PERFORMING ORGANIZATION REPORT NUMBER
ARL-SR-0346

9. SPONSORING/MONITORING AGENCY NAME(S) AND ADDRESS(ES)

10. SPONSOR/MONITOR'S ACRONYM(S)

11. SPONSOR/MONITOR'S REPORT NUMBER(S)

12. DISTRIBUTION/AVAILABILITY STATEMENT
Approved for public release; distribution unlimited.

13. SUPPLEMENTARY NOTES
POC: William O Coburn

14. ABSTRACT

There is an increasing interest in the use of reverberation chambers with mode mixing for testing of electromagnetic susceptibility and immunity of a device under test because of its repeatability and measurement speed. A reverberation chamber is characterized as an environment with uniform, randomly polarized, isotropic fields throughout the volume of the chamber over a large range of frequencies. These chambers are of particular importance because they improve the speed of acquiring shielding and coupling measurements. There have been multiple reports on the use of mode stirred chambers, but they are often inconsistent. The objective is to correlate the characteristics of the reverberation chamber to other facilities currently in use. The US Army Research Laboratory has constructed a medium-sized reverberation chamber (1.75 m x 2.55 m x 4.25 m); its preliminary characterization and calibration are described in this report.

15. SUBJECT TERMS
Reverberation chamber, isotropic, uniform

16. SECURITY CLASSIFICATION OF:			17. LIMITATION OF ABSTRACT	18. NUMBER OF PAGES	19a. NAME OF RESPONSIBLE PERSON
					William O Coburn
a. REPORT	b. ABSTRACT	c. THIS PAGE			19b. TELEPHONE NUMBER (Include area code)
Unclassified	Unclassified	Unclassified	UU	36	(301) 394-2705

Standard Form 298 (Rev. 8/98)
Prescribed by ANSI Std. Z39.18

Contents

List of Figures

List of Tables

Acknowledgments

I thank William O'Keefe Coburn for teaching things I never knew, as well as helping me master things I was only average at. Your time, effort, and patience, helped me understand more than I could have ever hoped to learn in such a short time period. Thank you Arthur Harris for constructing the antennas necessary to complete this report. I thank Neal Tesny for assisting with the development of the LabVIEW code and Timothy Burcham for writing the description and constructing the reverberation chamber.

1. Introduction

The need to decrease required testing times of electromagnetic susceptibility for electrically large devices or unmanned aircraft systems has led to a baseline characterization of the reverberation chamber at the US Army Research Laboratory (ARL). A multi-moded chamber allows for random polarization from every angle in a uniform isotropic environment, which highlights susceptibility and vulnerability due to a continuous wave frequency. The wavelength of interest on a particular device can be taken from the reverberation chamber, and then applied to the same device inside another facility, such as a gigahertz transverse electromagnetic (GTEM) or fully-anechoic chamber for further categorization.

An acceptable definition of a multi-moded chamber is one where the different modes become indistinguishable from one another, such that for any point inside the volume the modes will add coherently in space to yield a relatively uniform field throughout the volume. The dimensions of the chamber must be large compared to the wavelength of the frequencies in use in order to be properly multi-moded. It can also be assumed that the field lines achieve their maximum and minimum E and H fields on the walls, respectively.[1] Using the equations from Crawford and Koepke,[2] at 1500 MHz, there was over 19000 available modes. Mode excitation is achieved through the stirring of an aluminum paddle inside the chamber, which changes the boundary conditions.

$$\text{Number of modes} = \frac{8\pi}{3}\frac{VOL}{\lambda^3} \tag{1}$$

For 500 MHz,

$$\frac{8\pi}{3}\frac{18.97\text{m}^3}{(0.6\text{m})^3} = 735 \text{ modes}$$

For 1000 MHz,

$$\frac{8\pi}{3}\frac{18.97\text{m}^3}{(0.3\text{m})^3} = 5886 \text{ modes}$$

For 1500 MHz,

$$\frac{8\pi}{3}\frac{18.97\text{m}^3}{(0.2\text{m})^3} = 19865 \text{ modes}$$

Obtained parameters of interest were the peak to average (P/A) ratio; the Stirring Ratio (SR), which was a measure of maximum – minimum; as well as the standard deviation of the mean. It has become common practice to define the effectiveness of the chamber with the widely accepted Q-factor. This factor can only be written in terms of stored energy in relation to power lost, thus the instantaneous fields within the volume must be well characterized.[3] The formula for total energy inside the chamber is defined such that the fields are in phase throughout the entire volume and can be added together incoherently to acquire a total energy for the chamber[4] so

$$Q = 2\pi \frac{W_{stored}}{W_{dissipated\ per\ cycle}} = 2\pi f \frac{W_{stored}}{Power_{lost}} \qquad (2)$$

Equation 3 has been adjusted from its original author.[5] For the energy stored in a roughly uniform field, when adjusted for root mean square (RMS) values, the value of stored energy is

$$W_{stored} = W_e + W_m = 2W_e = 2\left[\frac{\varepsilon}{2}\iiint_V |E|^2\, dv\right] = \varepsilon_0 VOL|E|^2 \qquad (3)$$

The wave impedance inside the chamber is assumed to be that of a plane wave in free space, 120π Ω.[4] It has been previously established in that increasing either the number of paddles or the size of the paddle will improve the desired effect of the chamber, because the volume that is cut by the paddle will, in effect, change more of the boundary conditions. It has also been asserted that with a decrease in wavelength, the agreement between the modeled free space plane wave and the actual wave impedance inside the chamber will also improve.[6]

In order to demonstrate the uniformity of the field values, data were collected on the floor as well as elevated on a 2-ft polystyrene block. The Q-factor of the chamber was also compared between being free of lossy materials and under load by roughly cubic and rectangular blocks of absorber with volumes of 0.032 and 0.027 m^3, and surface areas (SAs) of 0.6069 and 0.7019 m^2, respectively.

2. Testing Facility

The reverberation chamber is characterized by brazed aluminum and brass with dimensions A x B x D as (1.75 x 4.25 x 2.55) m for a volume of 18.97 m^3. The chamber was meticulously designed with the intention of not perturbing the fields inside and allowing for proper multi-moding frequencies in the megahertz range or higher. The predominant factor in the wall material selection was to not introduce additional losses at the wall boundary, which requires a relative permeability of close to 1. The chamber was to be transported from the Aberdeen Proving Grounds to the ARL Adelphi site, which demanded the use of metal fasteners in order for it to be easily deconstructed. The metal sheet is 0.210 inches in thickness. All of the joints employed ¼ inch x 20 thread per inch bolts, made of either bronze or brass depending on the vendor. A bolt spacing of 2 inches was selected to both minimize the risk of bubbling of the skin and still remain producible.

There are approximately 3,200 bolts used to attach the structure together. All of these fasteners had to be drilled, countersunk, and tapped. All of the internal seams, joints, and any other imperfections were welded by a chosen vendor who chose the gas metal arc welding (GMAW) or inert gas wire feed process. The stirrer was then installed vertically, using brass bushings and an aluminum shaft at the opposite end from the door of the chamber. Power for the stirrer is supplied from a DC torque motor coupled to a speed reducing, right angle gear box. The motor is computer controlled and is able to position the stirrer to a minimum of 3,600 steps per revolution as well as hold the stirrer in the desired location or drive it through multiple turns as required. A zeroing point was equipped with a sensor and allows operators to quickly determine "home" position of the stirrer, but the feature has yet to be implemented. The chamber dimensions are shown in Figs. 1 and 2. The chamber block diagram is shown in Fig. 3, with the equipment list in Table 1. Figures 4, 5, and 6 are of the full loop, half loop, and Vivaldi antennas, respectively. Figure 7 is the Vivaldi antenna in position 2, transmitting into the corner of the chamber. Figure 8 is of the wall panel that allowed for the cables inside the chamber to connect to the proper equipment on the other side of the walls. Figure 9 is of the testing equipment setup and shows the radio frequency (RF) synthesizer, vector network analyzer (VNA), power meters, and the motor's DC power supply. Figure 10 is of the paddle stirrer. Figure 11 displays the 3 transmit positions while the receiver was held constant. Figure 12 shows several receiver positions while the transmit antenna was held constant in transmit position 2.

Ports not in use at the time of testing were terminated from the inside with shorts to prevent power leakage. This facility is a good example of a medium-sized cavity; however, these tests can be applied to chambers of a smaller volume.

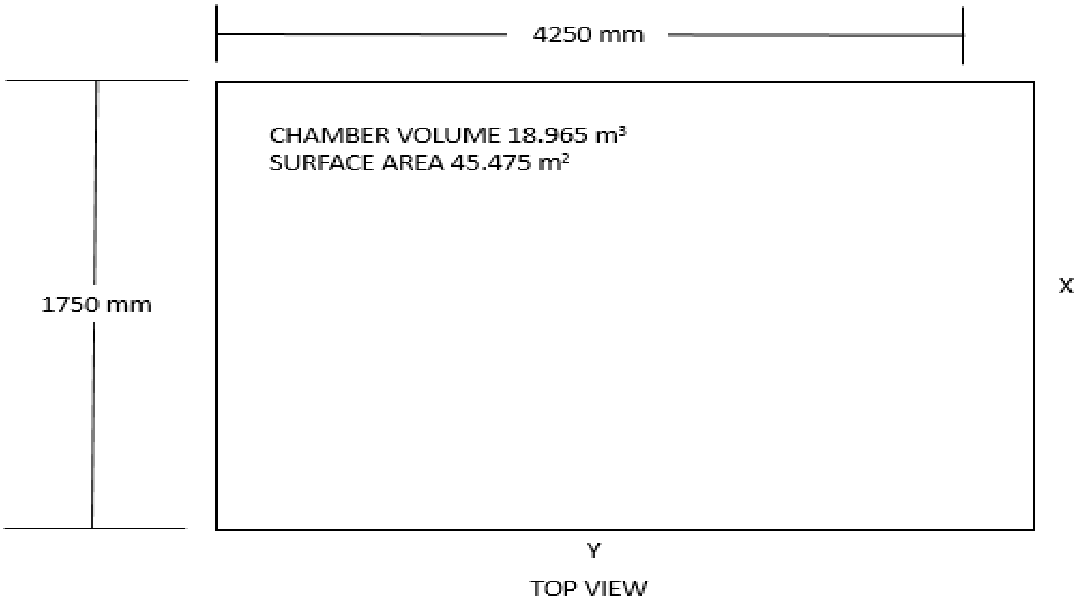

Fig. 1 Top view of the test facility

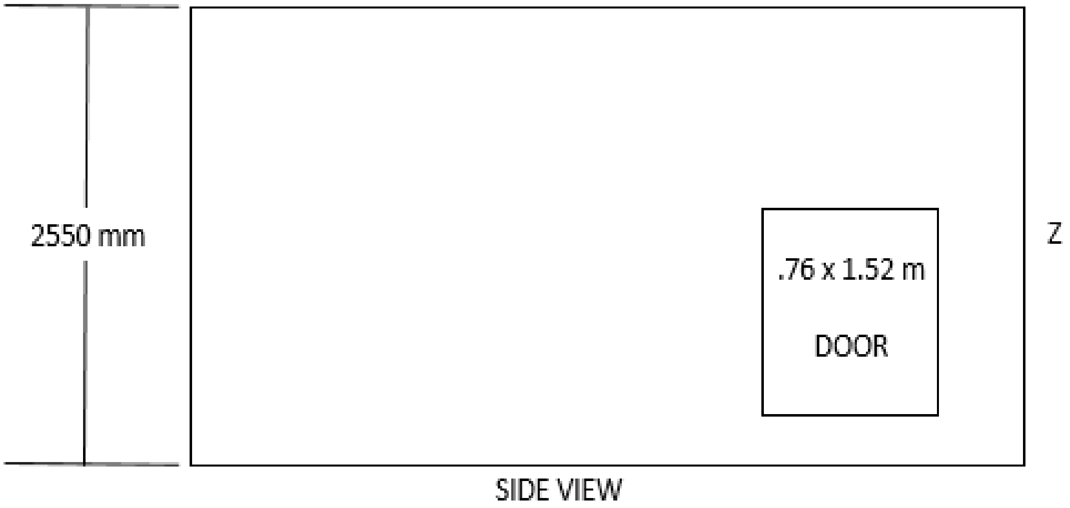

Fig. 2 Side view of the test facility

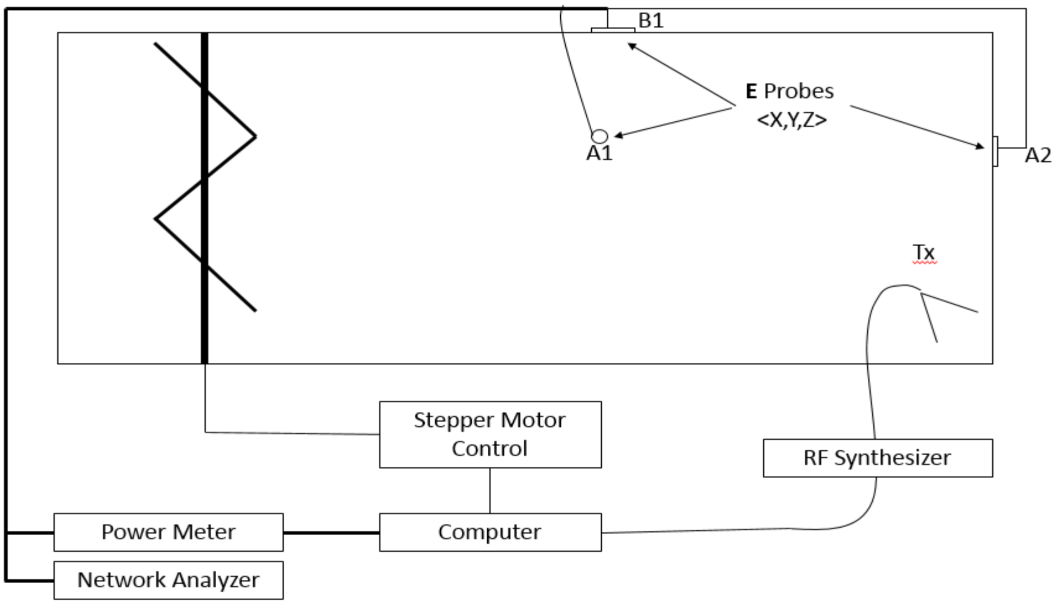

Fig. 3 Test setup top view

Table 1 Equipment used in testing

Equipment	No.	Model
Agilent Technologies System DC Power Supply	1	N5766A
Anritsu Vector Network Analyzer	1	37269NV
Gigatronics Universal Power Meter	2	8542C
Gigatronics Power Sensor	4	80303A
Anritsu Signal Generator	1	MG3692B
Wiltron RF Swept Synthesizer	1	6747B -20
Vivaldi Monopole Hybrid Antenna with 5-inch Ground Plane	2	
Half Loop Receiver with 3” Ground Plane	1	
Full loop Receiver with no Ground Plane	1	

Fig. 4 Standard SMA connected full loop receiver

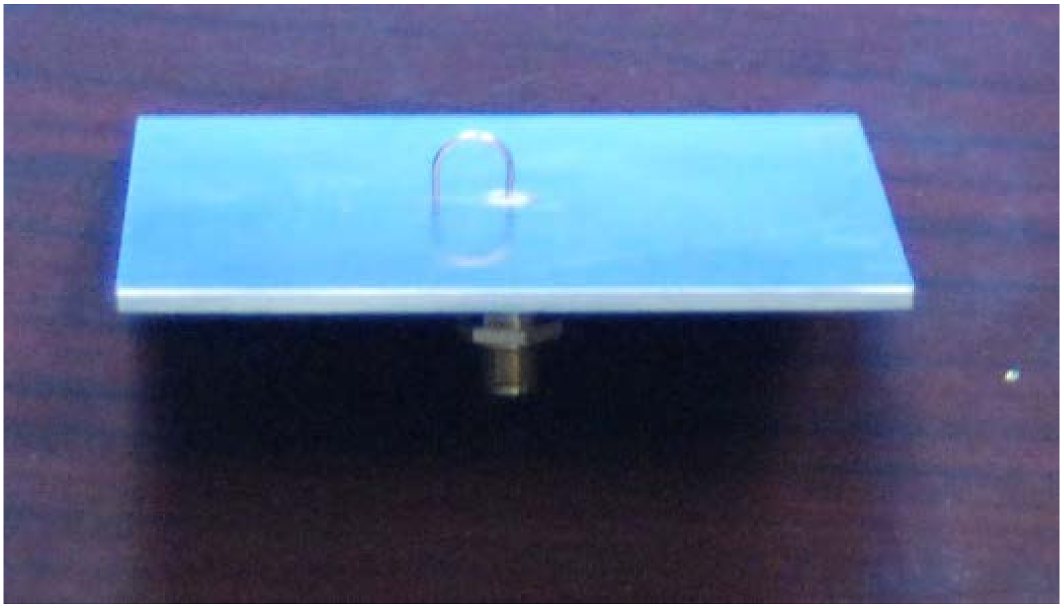

Fig. 5 Standard SMA connected half loop receiver

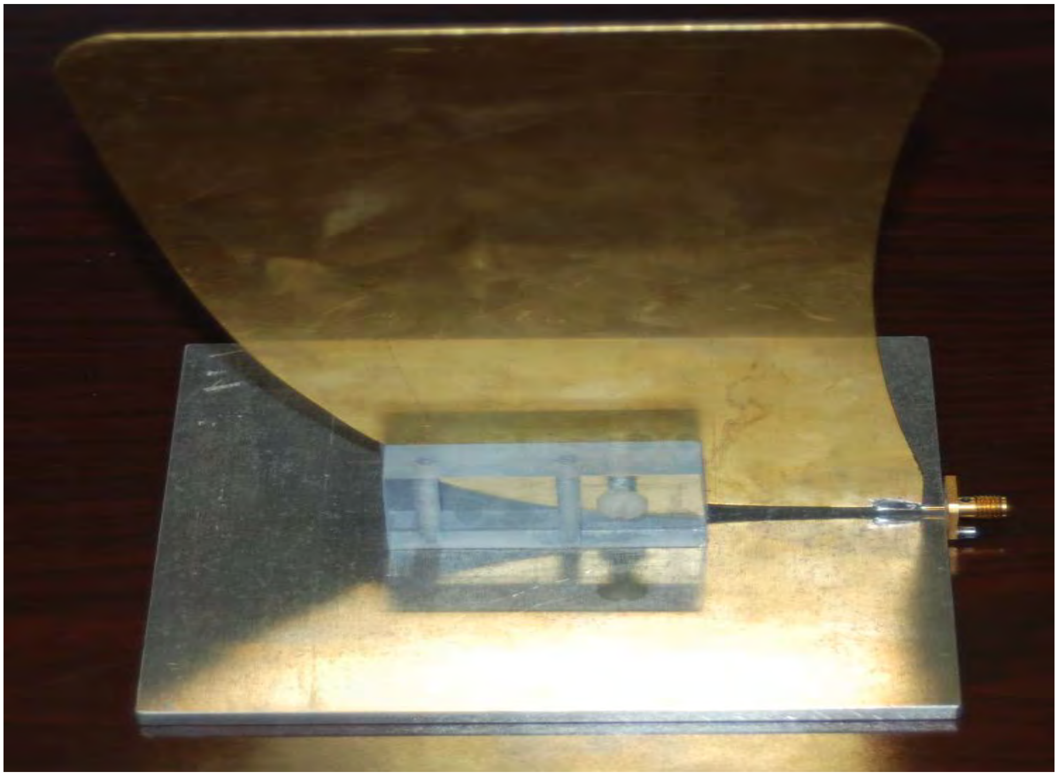

Fig. 6 Standard SMA connected Vivaldi antenna

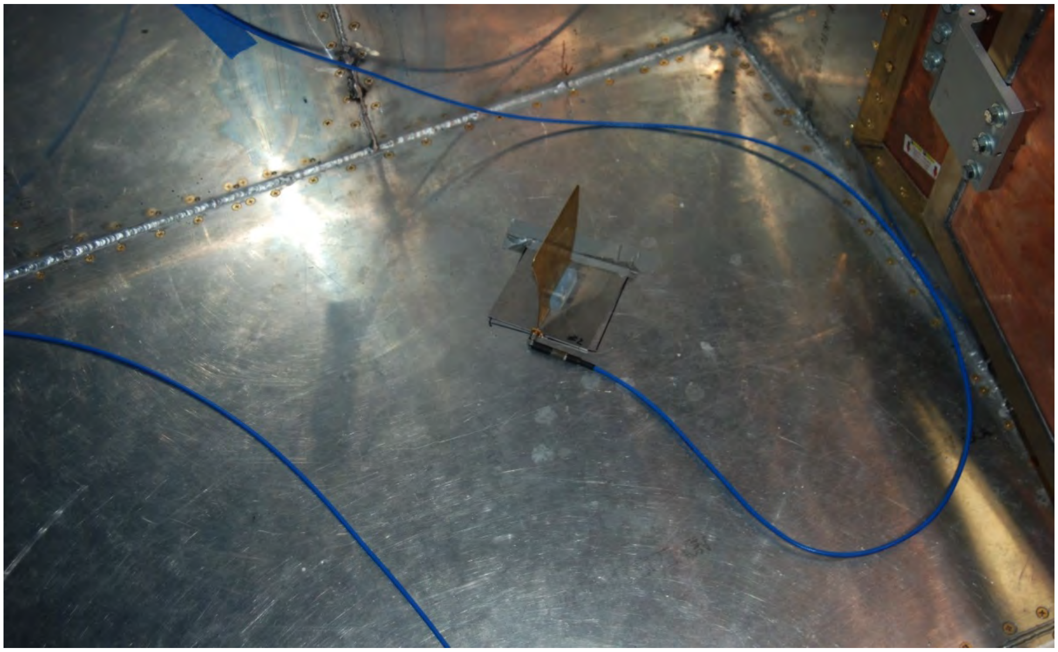

Fig. 7 Vivaldi antenna transmitting from position 2

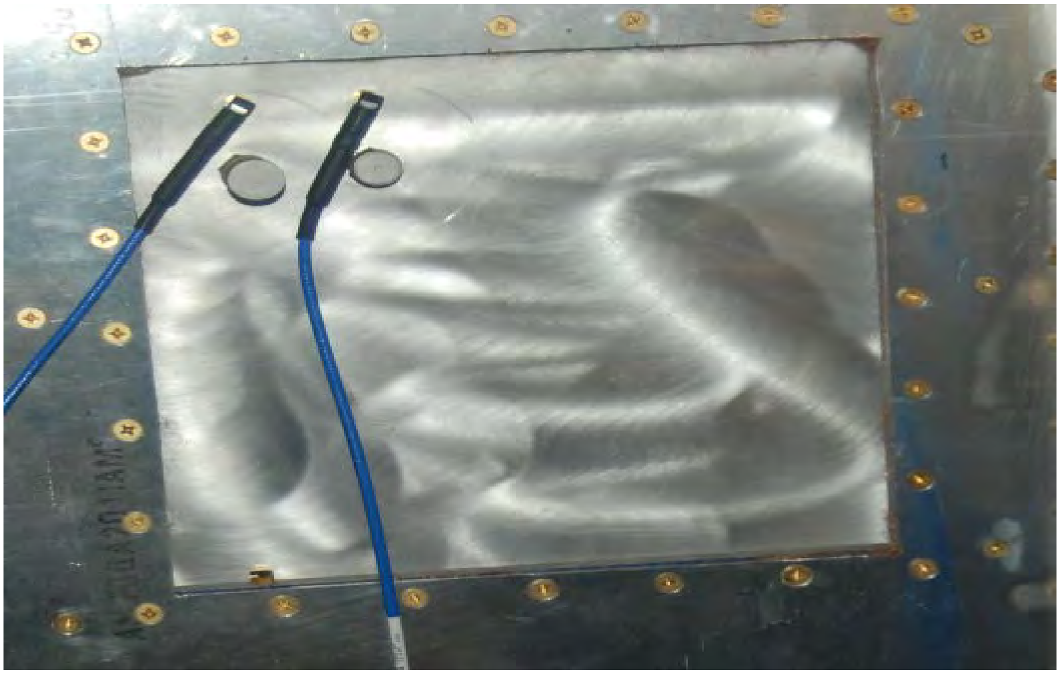

Fig. 8 Panel for ports to feed into the chamber

Fig. 9 RF synthesizer, VNA, power meters, and DC power supply

Fig. 10 Paddle stirrer

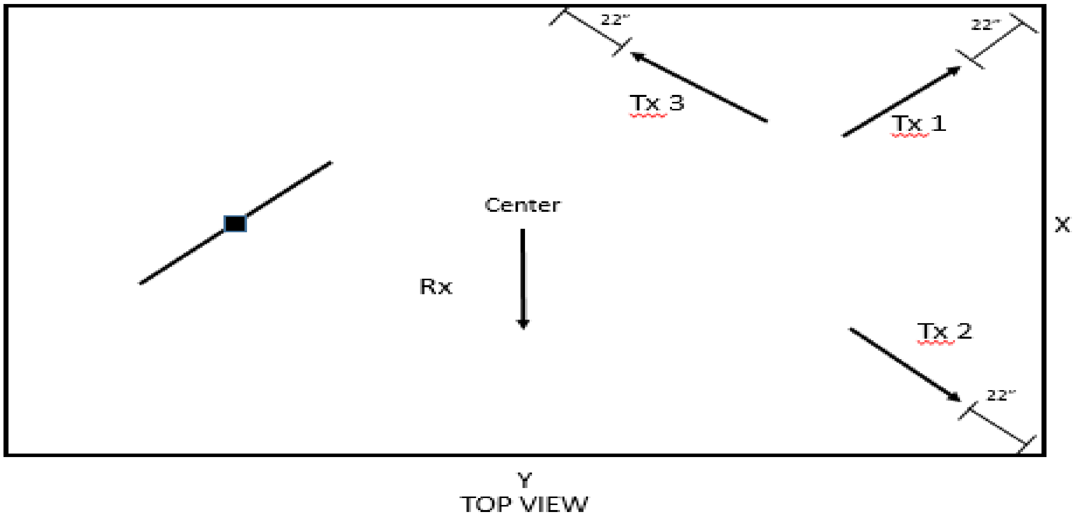

Fig. 11 Transmit and receive positions

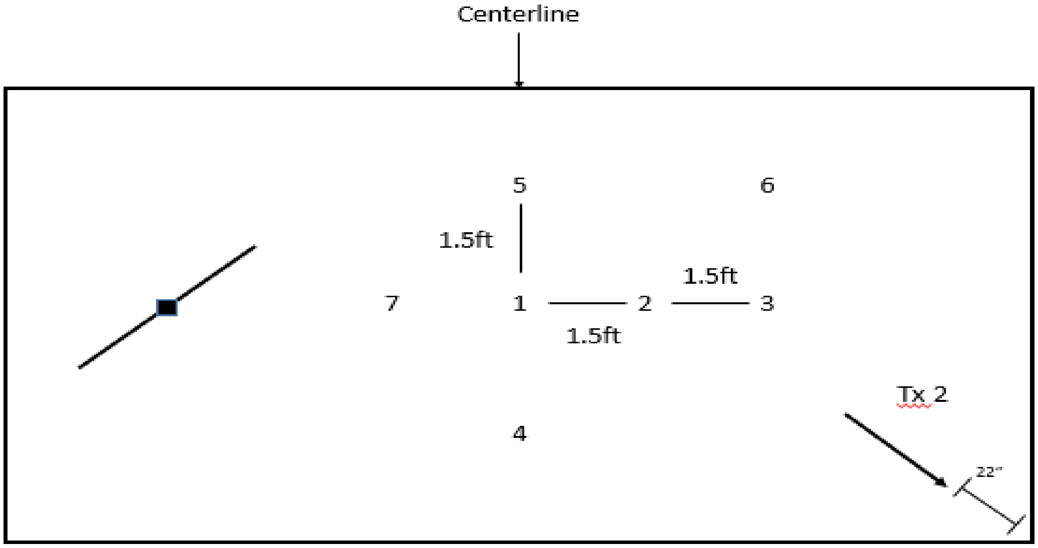

Fig. 12 Multiple receiver positions inside the chamber

Several receive positions were observed, while a single transmit position was used in order to demonstrate the uniformity in measurements.

3. Testing Calibrations

The transmit and receive antennas used inside the cavity were standard SMA and connected to the VNA through a 50-Ω cable, which was carefully calibrated using a full 12-term calibration for the collection of S-parameters, using the standard short open loaded transmission terminations. The voltage and magnetic field probes were connected directly to power heads through K-connector to SMA attachments, and then through a 20-ft cable to the power meters. The power meters where then zeroed by sealing the chamber, while no input signal was placed inside the chamber. This procedure was completed before every test. The theoretical value of the chamber Q-factor is given by Eq. 6, it can be assumed that for most nonferrous metals, μ_{rel} can be assumed to be 1.[7,8]

$$Q_{ant} = \frac{16\pi^2 * VOL}{\lambda^3} \tag{4}$$

$$Q_{wall} = \frac{3 * VOL}{2 * \mu_{rel} * SA * \delta} \tag{5}$$

$$\frac{1}{Q} = \frac{1}{Q_{ant}} + \frac{1}{Q_{wall}} \tag{6}$$

where

$$\mu_{rel} = \text{ relative permeability of the wall}$$

$$\text{SA} = \text{Surface Area of the Cavity } (\text{m}^2)$$

$$\delta = \sqrt{\frac{2}{\omega\mu\sigma}} = \text{skin depth (m)} \tag{7}$$

$$\sigma = \text{Conductivity of aluminum} = 3.7 \text{ x } 10^7 \, \frac{Siemens}{m}$$

$$\mu_0 = 4\pi * 10^{-7} \, (\frac{\text{Henrys}}{\text{meter}})$$

$$\omega = \text{radian frequeceny of operation (Hz)}$$

The first step is to know how much power is entering the chamber through the transmit antenna. Power reflected back to the source by the transmitter antenna must be measured by a VNA over the frequency range that was intended for data collection. The S_{11} of the antenna was measured over 3 different positions within the chamber and found to be consistent; reflections measured from inside the chamber yielded heavy spiking. The antenna used to transmit power into the room was a wide-band Vivaldi–monopole. There were 2 copies of the Vivaldi antenna, with slight variations from each antenna due to human error in construction. As represented in Fig. 13, the 2 antennas are near perfect copies of each other. To acquire presentable data, measurements were also collected inside a fully anechoic chamber.

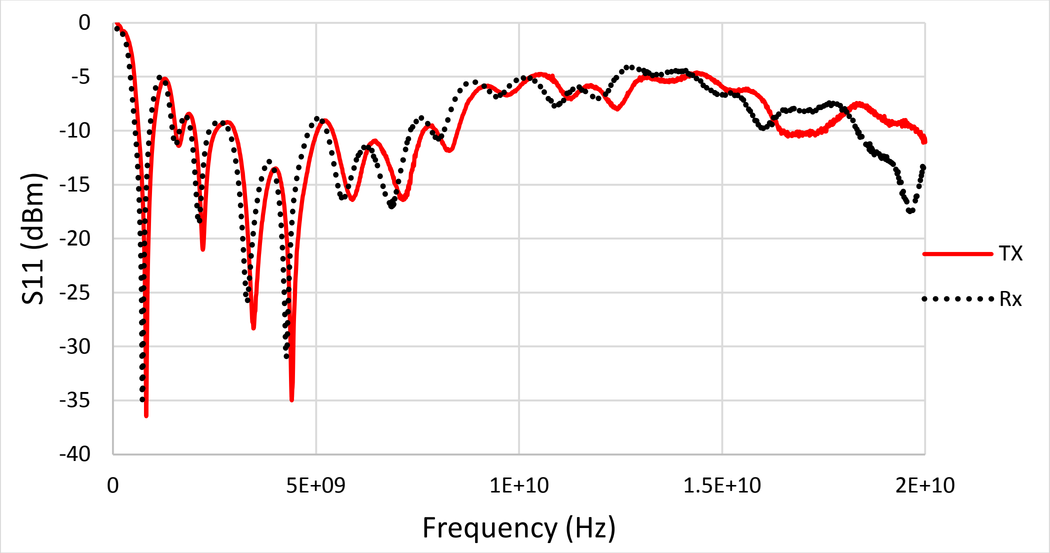

Fig. 13 $\quad$ **S_{11} of the transmit and receive antennas inside an anechoic chamber**

Not all the power from the RF synthesizer enters into the chamber due to reflections from impedance mismatch. A correction factor must be used to calculate how much power is actually being transmitted into the chamber. The antenna inside the reverberation chamber was directed to initially reflect off a wall and then toward the paddle to allow the wave to reach a steady-state before reflecting off of the paddle. Power that is generated by the RF synthesizer is not the same as what is transmitted by the antenna. A forward power reflection coefficient, Eq. 8, is applied to the power from the RF synthesizer to yield the actual power that is transmitted by the antenna. Power that is observed by the power meter must take into consideration the power that is reflected from the interface of a poorly matched receiver, as well as the 50-Ω power head. Equation 9 produces a fraction of the forward power that is actually present at the receiver. S represents the reflection coefficient magnitude and phase for a load.[10]

$$\frac{P_{Forward}}{P_o} = (1 - |S_{11}|^2) \tag{8}$$

where

$$P_{Forward} = \text{ Power that was Trasmitted (watts)}$$
$$P_0 = \text{ Power from the synthesizer (watts)}$$
$$P_{measured} = P_{actual}\,\frac{(1-|S_{meter}|^2)((1-|S_{receiver}|^2)}{|1-S_{meter}S_{receiver}|^2} \tag{9}$$

4. Testing Configurations

Power was then measured at the walls with voltage field probes, and then again with the full and half loop magnetic field probes, on the floor and throughout various places in the test volume. Testing commenced in a volume free of lossy materials such as absorbers. The paddle stirrer was spun at a rate of 15 RPM, the maximum for stirrer stability. An input signal was placed inside the chamber by the use of a transmit antenna. It was decided that since there are no discernable differences between transmit positions, the 2nd transmit position would be a constant while the receiver position was varied. The voltage probes were connected to 50-Ω power sensors, and then relayed to the power meter via a 20-ft DC cable. Three available receivers were connected to a 16 ft, 50-Ω coaxial cable, which was then feed through a wall panel and delivered to the 50-Ω power head. The triggering of data buffering from the power meters was set to be a group execute trigger, instead of an external trigger. Thus, data collection was initialized from a random initial starting paddle position every time. The power meters initially buffered 1000 points of continuous wave over a period of 8 s, which consists of 2 full rotation periods for the stirrer. It was determined that the same accuracy could be achieved as long as the paddle went through at least 1 full cycle. Data were then collected for 525 points over 4.2 s, yielding slightly more than 1 full rotation. This increased rate of gathering proved to yield no effect on the average value of power absorbed by the probes and was reflected in the standard deviation of the mean, as well as the P/A, SR, and Q-factor calculations.

The manual for the power meters specified a settling time of far below 2 ms, though not explicitly expressed. To avoid data misrepresentation, the time between data captures was set to a fastest rate of 4 ms. Prior to every data collection, the power meters were zeroed. The power heads were rated for a dynamic range of –70 to 23 dBm. In order to differentiate between real and questionable data, all recorded values below –69 dBm were replaced with the value –69 dBm. This replacement filtered out false readings given by the power meters to obtain an accurate noise floor reading. This inherently contributes to slight error in averaging of power levels in the data. To mitigate this, power was transmitted into the chamber at 16 dBm. In addition, magnetic field probes with a higher transfer function than voltage probes were used. The control of experimentation parameters, as well as collection of data was completed via computer through a GPIB cable and the use of LabVIEW (http://www.ni.com/labview). For each period of collection, a monochromatic frequency entered the chamber and was then incremented by 100 MHz along the range of 500–6000 MHz. The automation of this system enabled in-situ observation of stirrer position error in number of steps, as well as how the electric field was changing from the wavelength involved. The 3 orthogonal precision machined short monopole voltage probes where placed at irregular intervals offset from center on each wall and an empirical polynomial transfer function was applied to each probe to convert measured power to a realizable electric field, as given by

$$Transfer\ Function = \frac{\frac{V}{m}}{Volt} = \frac{\sqrt{Z_{LOAD} * Power_{measured}} * \sqrt{(Z_{Load} + Z_{real})^2 + Z_{imaginary}{}^2}}{Z_{Load} * H_{Eff}} \tag{10}$$

$$H_{Eff} = \text{Effective Height of The Voltage Probes (m)}$$
$$Power_{measured} = RMS \text{ Power seen by The Probes (watts)}$$
$$Z_{Load} = 50\ \Omega \text{ Power Head}$$

$$E_{measured} = \frac{V_{oc}}{H_{Eff}} = \frac{V_{measured}}{H_{Eff}} \frac{\sqrt{(Z_{Load}+Z_{real})^2+Z_{imaginary}{}^2}}{Z_{Load}} \tag{11}$$

The apparent length of the voltage probe increased with frequency, until the length of 18 GHz, where the wavelength became small compared to the probe tip length (Fig. 14). In addition, the probe tip appeared as a short at lower frequencies started to appear as more of an open circuit as frequency increased.

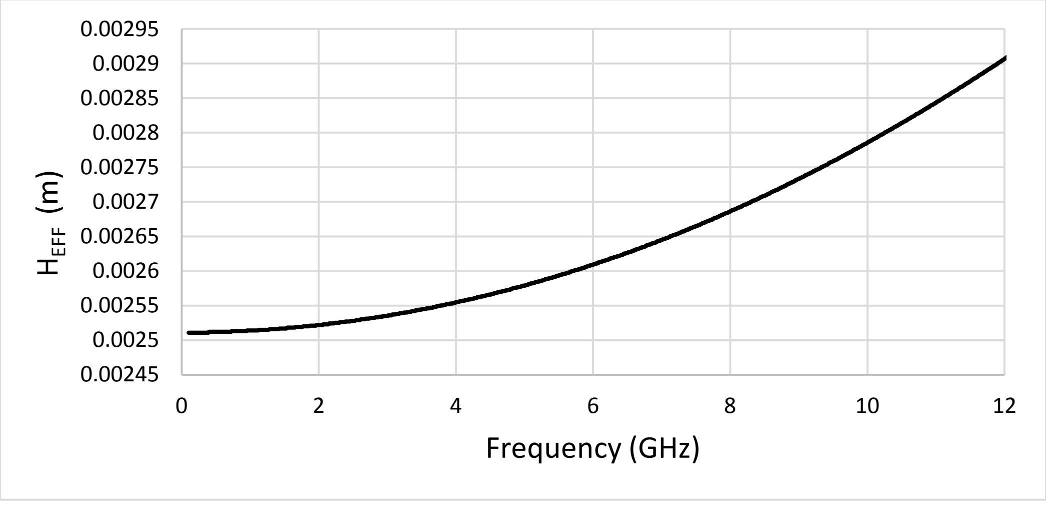

Fig. 14 Effective height of the voltage probes

Tests with the magnetic-field probes were also completed with a half loop probe backed by a (3 x 3) inch ground plane, as well as with a full loop probe of radius 0.125 ft. The increased capture area of the full loop was double that of the half loop, and correlated to a gain of 3 dBm for the fields from the half loop to the full loop, as to be expected. The impendence mismatch of the loop was not important because the open circuit voltage was calculated terminating into a high impedance.

$$V_{oc} = A\frac{dB}{dt} = j\omega A B_{meas} \tag{12}$$

$$B_{meas} = \sqrt{50 * Power_{measured}}\,\frac{(Z_{Load}+Z_{real})}{j\omega A Z_{load}} = \frac{E_{measured}}{c} \tag{13}$$

where c is the speed of light as $2.9979*10^8$ m/s

Figure 15 is a plot of the transfer functions for the different receivers that were used with respect to a single electric field only. It can be noted that the impendence matching is the primary cause for how effective the receiver is at capturing power.

The associated transfer functions for the wall probe receivers were determined empirically. The other antenna transfer functions were acquired with the assistance of FEKO (www.feko.info). Each transfer function is only presented with respect to the dominant electric field component into 50 Ω. This is a good approximation for the short monopoles, which only respond a single field component. Unfortunately, the other antennas respond to all the field components, the loop receivers respond to both the components that occupy its planar space. With this in mind, the other antenna's transfer functions could be improved by taking into account the other field components present.

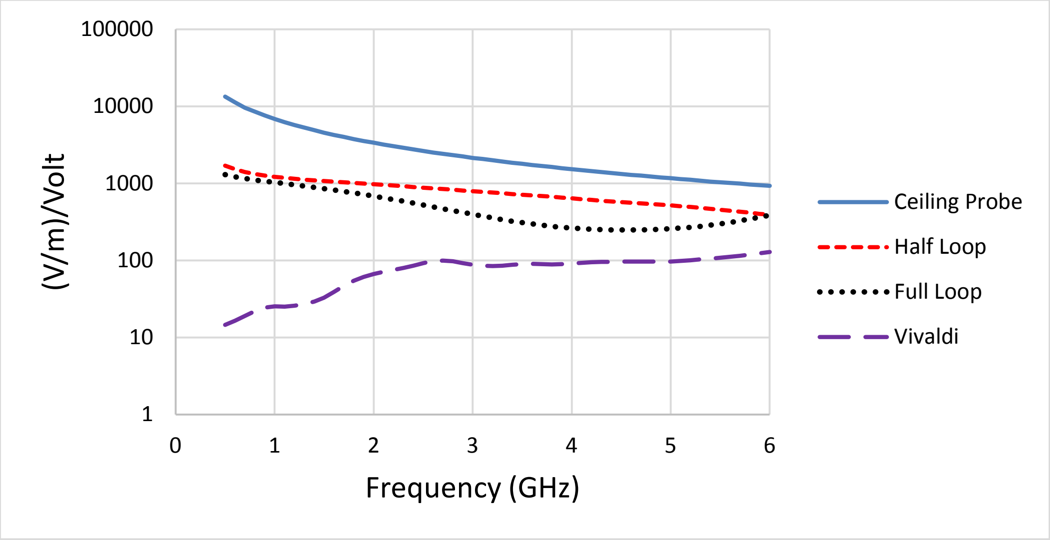

Fig. 15 Vertical transfer functions for all receivers

The magnetic field that was perpendicular to the loop plane was measured. This test was repeated 3 times to get the 3 components while on a 2-ft polystyrene block. While collecting data, a high gain horn antenna was used near gaskets to detect leakage of power through small gaps, which consistently measured below –60 dBm. The electric fields calculated by each wall probe was derived from the power. Since power is incoherent, the addition of the electric fields must be treated as such. Using the equations found in Liu et al.[9] the cavity Q-factor of the chamber was only true at higher frequencies, assuming negligible spatial variations of the fields gives[3,10]

$$Q = \frac{2\pi\, f\, VOL\, \epsilon_0}{P_{in}} (E_x + E_y + E_z)^2 \tag{12}$$

where

$f = \text{Frequency (Hz)}$

$VOL = \text{A x B x D} \ \ (\text{m}^3)$

$P_{in} = \text{input power from transmit antenna (watts)}$

$\epsilon_0 = \text{Permitivity of free space in } (\frac{\text{Farads}}{\text{meter}})$

$E_i = \text{ Electric Field in direction i in } (\frac{\text{V}}{\text{m}})$

5. Results

The multiple transmit and receive positions were analyzed and compared as specified in Fig. 11, and it was conclusive that the Q-Factor, P/A, and SR on the walls were unaffected by the change of the transmit position inside the chamber as long as the first reflection did not come from the paddle itself. The Q-factor from 3 different transmit positions was calculated and plotted for each wavelength in Fig. 16. It can be observed that there is no distinguishable difference between the multiple transmit positions inside the chamber, as shown with the P/A in Fig. 17.

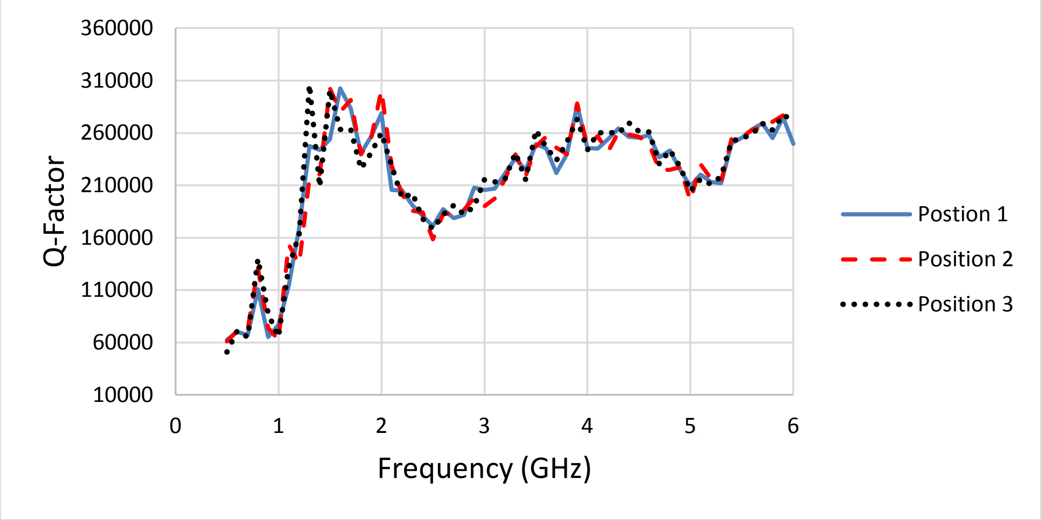

Fig. 16 Q-factor from the different transmit positions

Figure 17 is a plot of the P/A from wall probe located on the wall across from the door, A1, for the 3 transmit positions. The peak to average should be ~10 dB, indicating that most of the time the average receiver power is within an order of magnitude of peak value.

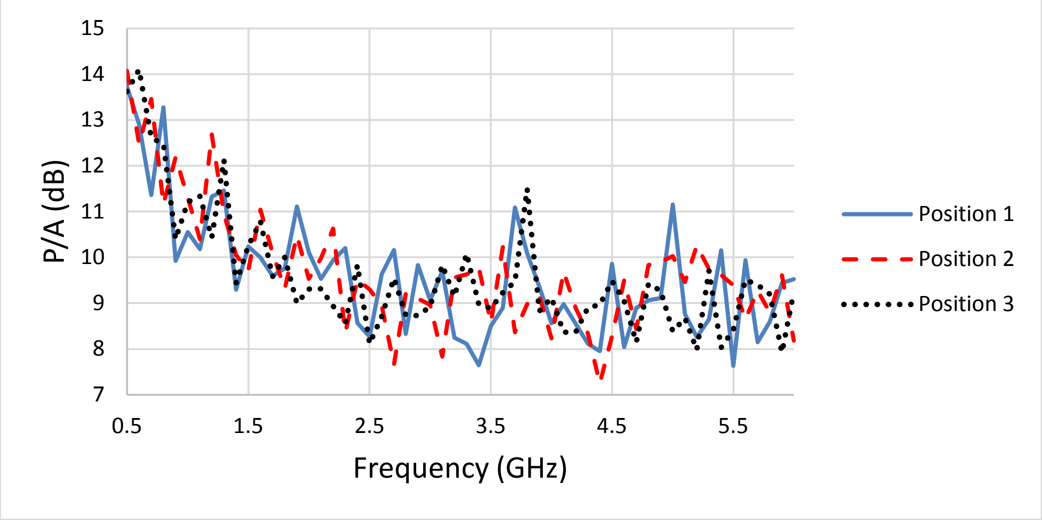

Fig. 17 Peak to average ratio from the different transmit positions

The stirring ratio gives insight into how the instantaneous field is changing. The SR is a measure of maximum to minimum receiver power and should be above 20 dB to be a sufficient chamber of reverberation.[7] The chamber proved to be valid over the entire frequency range of testing. Figure 18 is the SR associated with the probe on the ceiling, B1, while the transmitter was in positions 1, 2, and 3. The SR demonstrated in Fig. 18 is representative of the SR of all the probes for any antenna configuration.

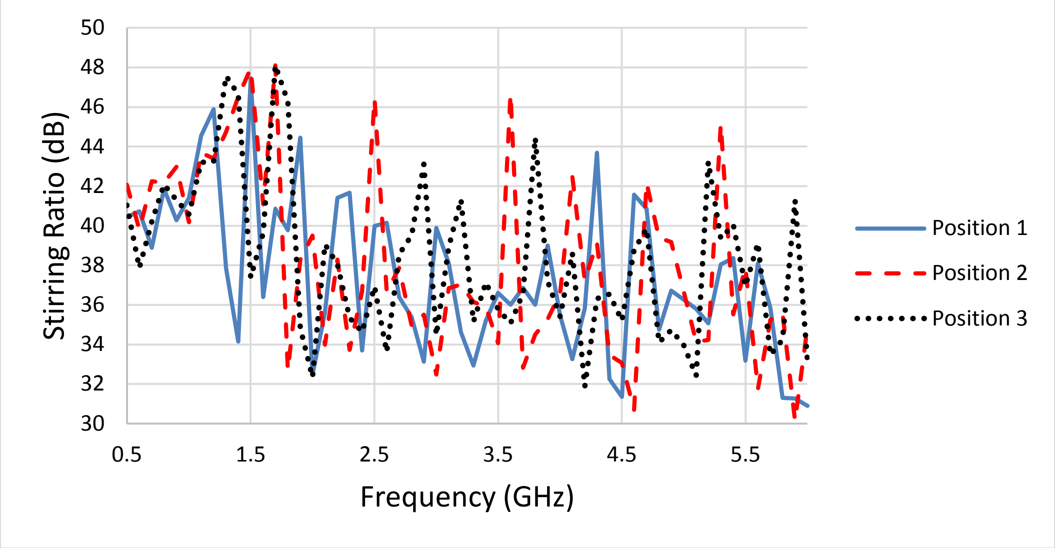

Fig. 18 Stirring ratio from the different transmit positions

In the region where the chamber becomes multi-moded, the spread in the data points shrinks. The value of the standard deviation between 1000 sample points was calculated and then normalized to the mean for the probe A1 in Fig. 19. The larger than 3 dB normalized standard deviation for frequencies below 2000 MHz is because of insufficient modes being present. Each curve demonstrates the systematic error seen by probe A1 from the 3 different transmit positions inside the chamber. Figure 19 can be interpreted as most of the data points are within 3 dB of the mean value. The theoretical value for this number is 3 dB, as found in Hatfield et al.[7] The standard deviation of the mean settles to an approximately constant value of just above 3 dB after 2000 MHz.

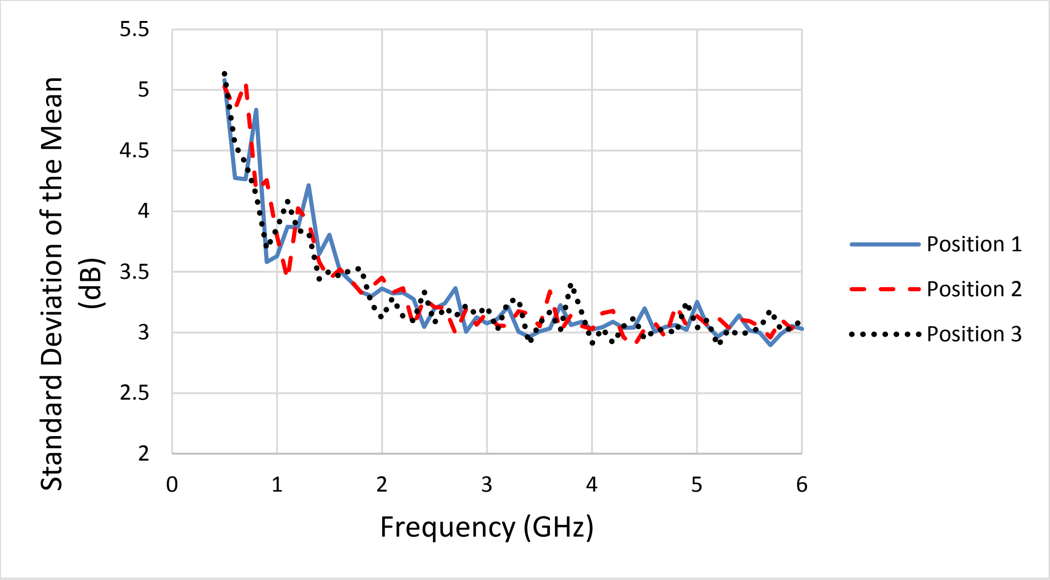

Fig. 19 Standard deviation of the mean for the different transmit positions

The values from Fig. 19 when sampled from 1000 points were found to be all most identical to the same tests under conditions when 525 points were taken, proving that only 1 full rotation is needed to acquire good data. Figure 20 is also a plot of the standard deviation of the mean associated with each probe while the chamber was empty and the transmitter was in position 2 over 525 points.

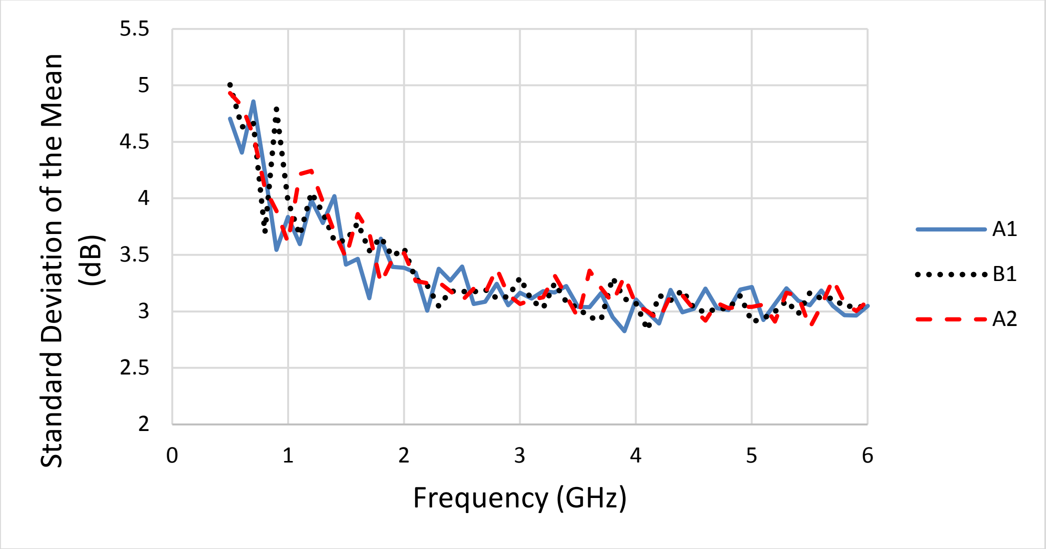

Fig. 20 **Standard deviation of the mean from for the different wall probes**

However, as far as uniformity is concerned, every experiment that was ran yielded similar results, which is characterized by the standard deviation of the mean. Tests of varying transmission and varying reception yielded similar results. Figure 21 shows how uniformly the results were when only varying the receiver position as well as when varying only the transmitter position. The values associated with the receiver were ones where the receiver was orientated to intercept the Y component of the magnetic field. The values associated with the transmitter were calculated from the standard deviation of the B1 ceiling probe.

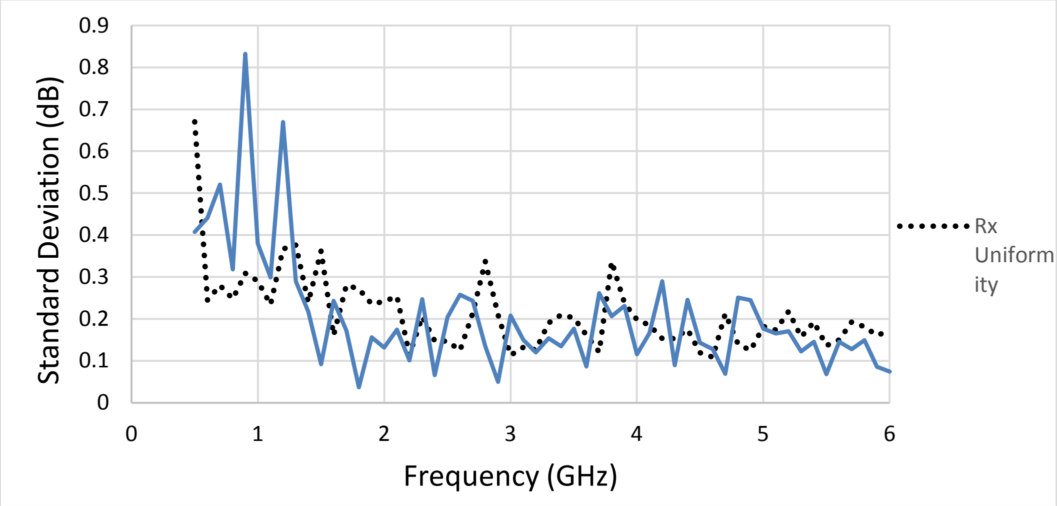

Fig. 21 **Uniformity of inside the chamber**

The power from each probe indicated that all the components on the chamber walls were equally distributed at the wall points. Figure 22 is a graph of the power received by the B1 probe, both with corrections and uncorrected. When the data were corrected, it was with respect to the power that the transmitter was able to transmit, using Eq. 8. Note how the corrections has little to no effect even when the Vivaldi transmitter is not well matched. The graph of Fig. 22 is typical of the power viewed from each probe, so only the B1 ceiling probe was displayed.

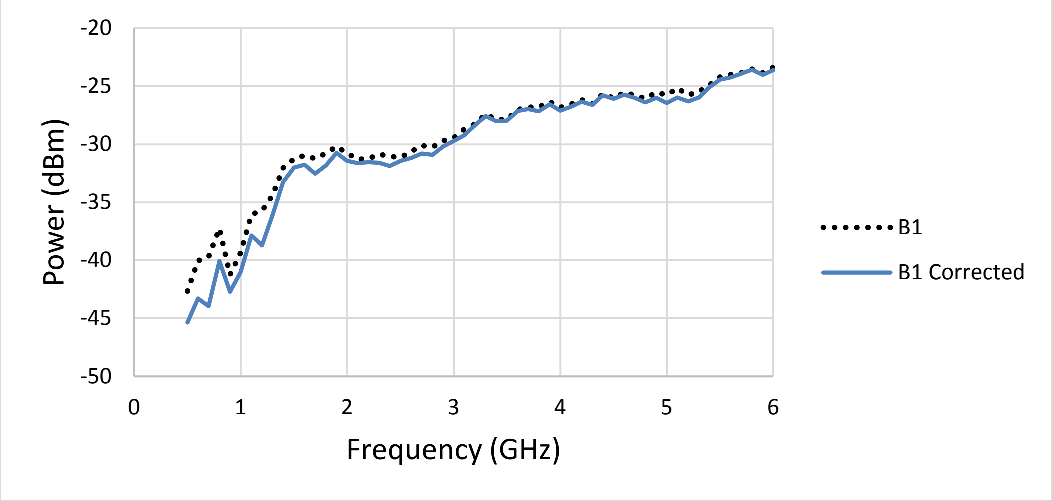

Fig. 22 Received probe power adjusted for input power

The fields inside the test volume were found to be consistent between 3 different orientations over 3 different tests on a 2-ft polystyrene block. This agrees with the theory associated with a reverberation chamber operating within the black hole region, defined as a chamber with enough modes to fill the volume to provide random polarization.[1] From the transmitter's orientation in position 2, the waves produced as a transmitter will be linearly polarized waves. Figure 18 depicts the 3 uncorrected orthogonal components from the Vivaldi as a receiver in receive position 1. Since the values of the field components are equivalent, the chamber must be producing equivalently random polarizations. The consistency between the 3 field components was found in the repeated procedures for the half and full loop receivers as well as when placed in receive position 6. This notion can be extended, the components are equivalent throughout the 7 tested receiver positions.

A correction factor can be applied to the power that is measured by a receiver, to what is actually displayed at the meter, from Eq. 9. This correction, when applied, can overestimate the measured field, so it was not applied. Figure 23 is the applied correction factor for the Vivaldi antenna. Its reflections as both a receiver and transmitter are symmetric, so when applied, they cancel because of reciprocity. Figure 24 shows the average power received.

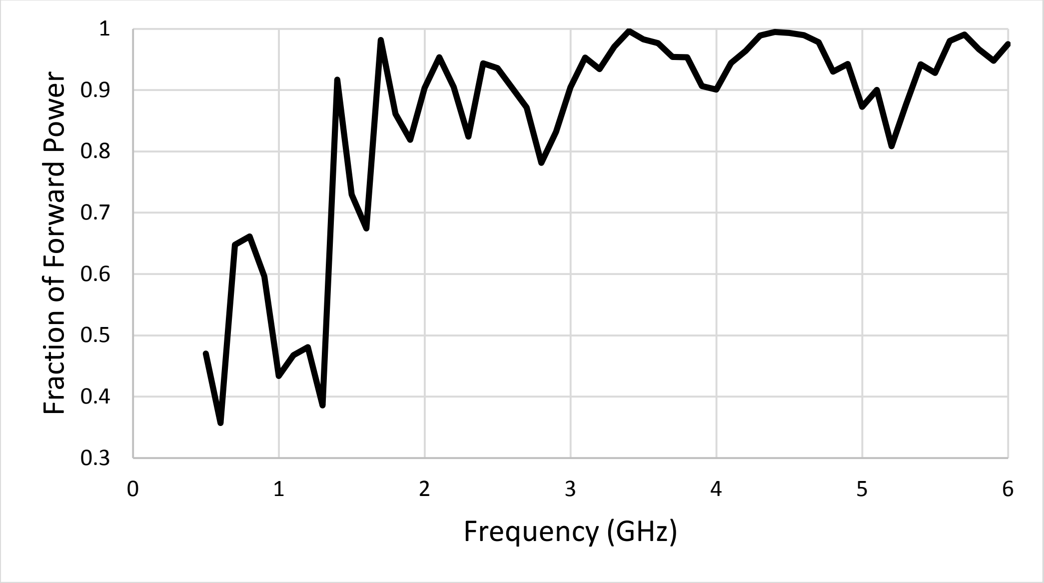

Fig. 23 **Fractional value of received power for the Vivaldi antenna**

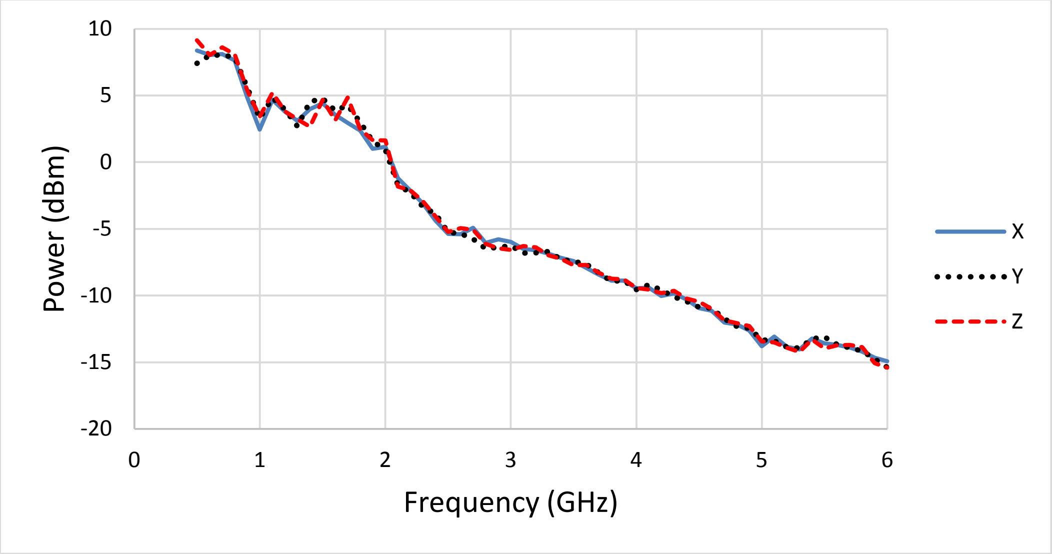

Fig. 24 **Average power received by the Vivaldi receiver on a 2-ft polystyrene block**

Figure 25 is a comparison of the theoretical value of the Q-factor from Eq. 6 versus the measured values from the use of Eq. 12. It can be observed that the 2 curves are very inconsistent.

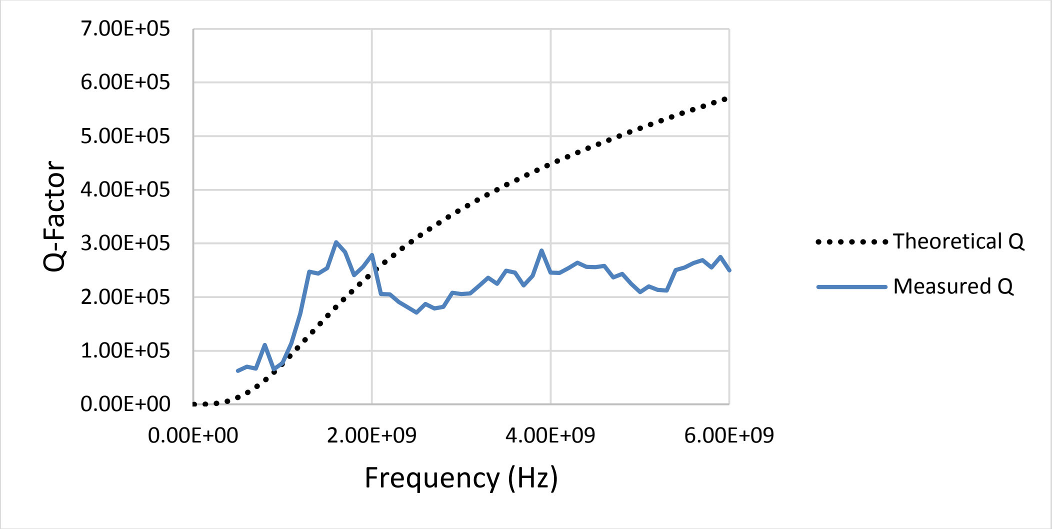

Fig. 25 Q-factor as a function of frequency

Several position's magnetic Y component values were measured with the full loop receiver and found to be indistinguishable within 1 dBm for frequencies above 1000 MHz. Figure 26 is the received power from the full loop oriented to intercept the Y component of the magnetic field over various receiver positions, when adjusted for the for power transmitted, from Eq. 8.

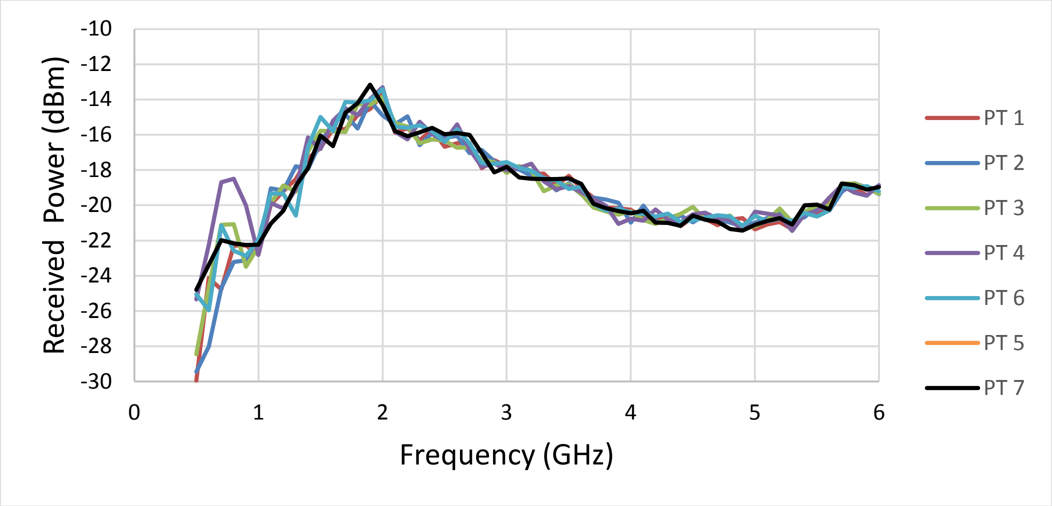

Fig. 26 Y component value of the magnetic field

A mean value of the received power in Fig. 26 was calculated for the 7 receiver positions, each position was then subtracted from this mean and then plotted in Fig. 27. After 1300 MHz, the difference from the mean is within 1 dB for all positions.

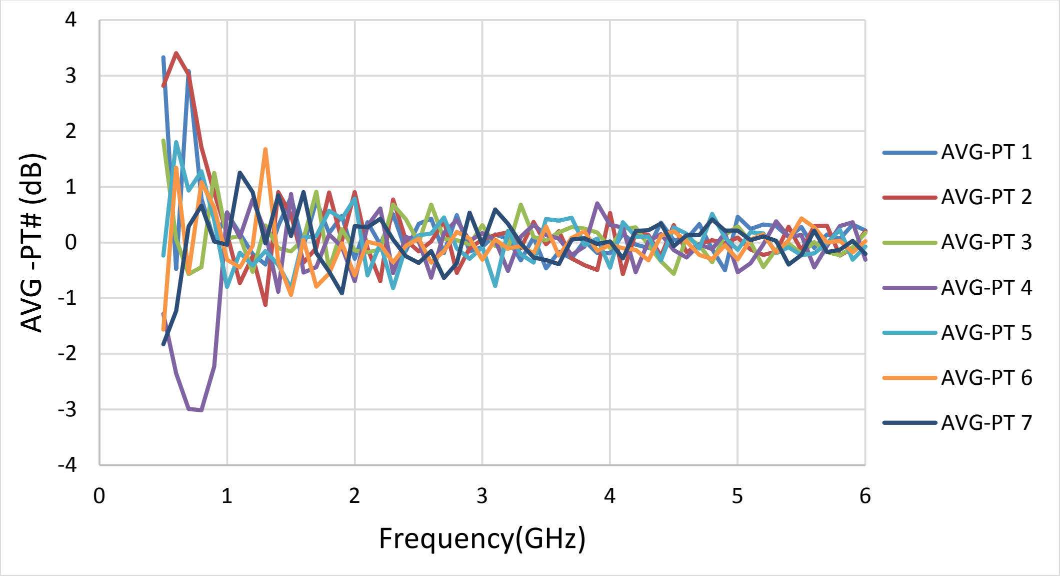

Fig. 27 **Mean power minus receiver position power**

The reduction of the Q-factor under load was compared with a rectangular block of absorber of 2.76*10^{-2} m^3 and a cubic block of volume 3.2*10^{-2} m^3. Both absorbers were placed on a polystyrene block of approximately 6.31 *10^{-2} m^3. The rectangular absorber was a placed lengthwise vertically to intercept more field lines, and in Fig. 28 it is apparent that both absorbers significantly reduced the Q-factor, but the rectangular block absorbed more power than the cube because it intercepted more field lines even though it was a smaller volume.

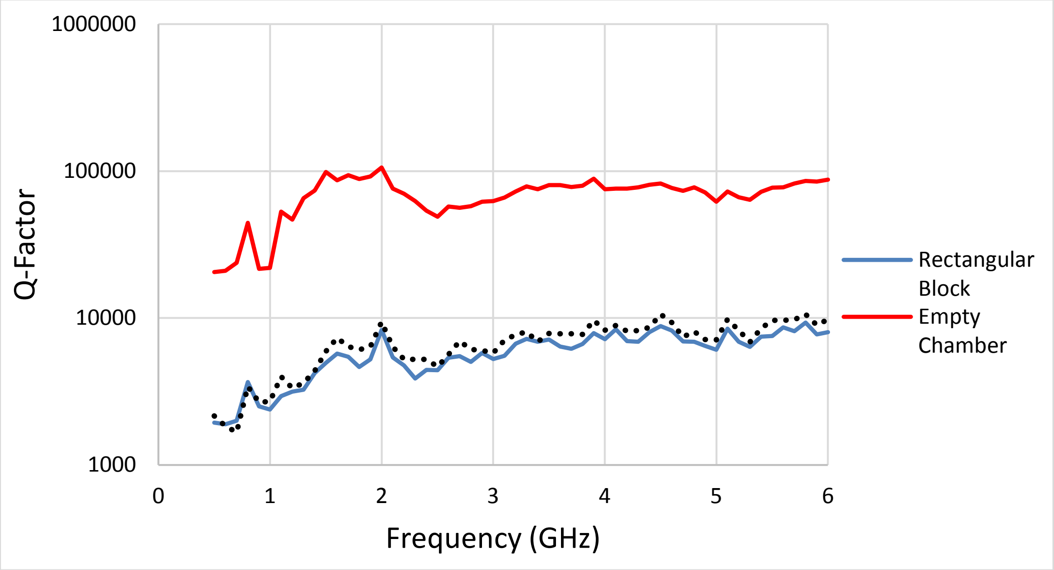

Fig. 28 **Chamber loaded vs. empty**

Figure 29 is a plot of the approximate power density seen by each receiver while 2 ft off the ground on a polystyrene block, the wall probe gives the best approximation of what is expected inside chamber on account of it has the best approximation of a transfer function. The full loop receiver suffers the greatest loss of accuracy because it lacks a ground plane, because time constraints, the transfer function associated with the loop receivers is incomplete with respect to all the components.

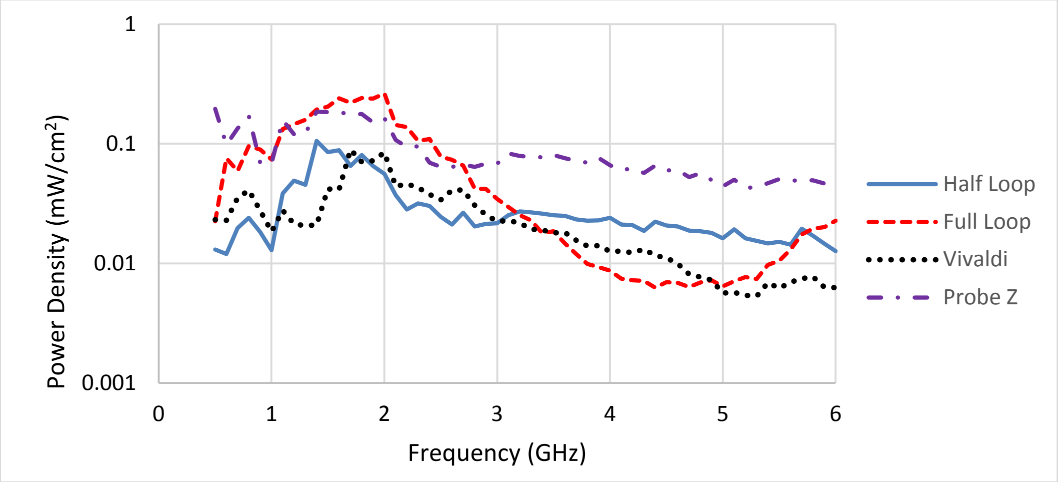

Fig. 29 Power density vs. frequency for the 4 different receivers

6. Recommendations

A higher power input signal power will help to increase the dynamic range and distinguish the data from the noise. A higher paddle stirrer angular velocity will decrease data collection time. Unused ports should be terminated from the inside with short circuits to prevent additional leakage. It would be beneficial, though time consuming, to collect data with 1 probe at a time rather than using 3 wall probes simultaneously.

It is recommended that all receivers and transmitters be placed disconnected inside the chamber for any given test of a baseline, loading effects from having equipment under test (EUT) inside the chamber are observable while testing.[2] The reason being is that an increased amount of metal will perturb more field lines and consequently give different values based on the amount present.

7. Conclusions

The evidence presented in this report concludes within measurement uncertainty, that for a reverberation chamber with a sufficiently large stirring paddle constructed of nonferrous materials, the presence of sufficient TEmn and TMmn modes does in fact create randomly polarized, uniform, isotropic fields inside the chamber. Furthermore, the standard deviation of the mean is about 3 dB for all frequencies above 2000 MHz with a uniformity below 0.9 dB for frequencies above 500 MHz. Most of the power inside the chamber is within 0.9 dB of the mean or better for any given frequency. This indicates that the chamber is ideal for testing at frequencies greater than 2000 MHz

For frequencies below 2000 MHz, the operator must adjust the data to acquire accurate readings of the fields inside the chamber. The Q-factor measured was lower than expected, this could be due to the slightly leaking gaskets as well as having 3 or more probes collecting data. The power density inside the chamber is about 0.05 mW/cm^2 over the test frequency range for a 40-mW input.

Having sufficient modes allows for indistinguishability with respect to polarization and uniformity, with this in mind, these characteristics do not become apparent until at least 2000 MHz, which is obvious from Fig. 15. Using Eq. 1, the minimum number of modes required to become sufficiently multi-moded in a chamber with the dimensions at ARL is

$$\frac{8\pi}{3}\frac{18.97\mathrm{m}^3}{(0.15\mathrm{m})^3} = 47085 \text{ modes}$$

The amount of modes present, which determines the operating point of the chamber, is ultimately dependent on the chamber wall sizes compared to the wavelength. The chamber wall sizes must be electrically large compared to the wavelength to be fully in the reverberation region. Using the frequency determined to be the beginning of the reverberation region, 2000 MHz, the volume of the chamber must be at least 5000 times larger than the cubic value of the wavelength.

8. References

1. Quine JP. Development of methodologies for electromagnetic susceptibility evaluation. Final Technical Report, Rome AFR Base, CALSPAN-UB, Rome, NY, RL-TR-96-43 March 1996.
2. Crawford ML, Koepke GH. Design, evaluation, and the use of a Reverberation chamber for performing electromagnetic susceptibility/vulnerability measurements. NBS Technical Note 1092, April 1986.
3. Corona P, Latiral G, Paolini E, Piccioili L. Use of a reverberating enclosure for measurement of radiated power in the microwave range. IEEE Transactions on Electromagnetic Compatibility. May 1976;EMC-18(2).
4. Corna P, Latiral G, Paolini E. Performance and analysis of a reverberating enclosure with variable geometry. IEEE Transactions on Electromagnetic Compatibility. February 1980;EMC-22(1).
5. Balanis Constantine A. Advanced engineering electromagnetics. New York: Wiley, 1989.
6. Corna P, Ladbury J, Latmiral G. Reverberation-chamber research-then and now: A review of early work and comparison with current understanding. IEEE Transactions on Electromagnetic Compatibility IEEE Trans. Electromagnetic Compatibility. February 2002.
7. Hatfield MO, Freyer GJ, Slocum MB. Reverberation characteristics of a Large welded steel shielded enclosure. Joint Warfare Applications Department, NSWCDD/TR-96/149, October 1996.
8. Loughry TA. Frequency stirring: An alternate approach to mechanical mode_stirring for the conduct of electromagnetic susceptibility testing. Final Report, PL-TR-91-1036, Phillips Laboratory, November 1991.
9. Liu BH, Chang DC, Ma MT. Eigenmodes and composite quality factor of a reverberation chamber. National Bureau of Standards (US) NBS Tech. Note 1066, August 1983.

1 DEFENSE TECH INFO CTR
(PDF) DTIC OCA

2 US ARMY RSRCH LAB
(PDF) IMAL HRA MAIL & RECORDS MGMT
RDRL CIO LL TECHL LIB

1 GOVT PRNTG OFC
(PDF) A MALHOTRA

2 US ARMY RSRCH LAB
(PDF) RDRL SER M
S A MCCORMICK
W O COBURN

INTENTIONALLY LEFT BLANK.